STRAIN INDUCED STRUCTURE TRANSITION IN HOT DEFORMED γ+α DUAL-PHASE TITANIUM ALUMINIDE①

Chen Guoliang and Wang Jinguo
State Key Laboratory for Advanced Metals and Materials, Department of Materials Science and Engineering, University of Science and Technology Beijing, Beijing 100083, P. R. China

ABSTRACT Strain induced structure transition (SIST) during hot deformation in TiAl alloy was investigated by high-resolution transmission electron microscopy(TEM). Various non-equilibrium asymmetrical twin boundaries with a large number of ledges were found. Special non-equilibrium tilt and asymmetrical γ/α interfaces were also illustrated. The normal crystal relation between γ and α can be changed. The 1/3[111] Frank partial dislocations often appear at these non-equilibrium interfaces. It was also reported that the strain induced phase transitions, including γ → α, α → γ and γ → 9*R* structure, commonly occur during hot deformation; the strain induced phase transitions are closely related to interface structure. The dislocation reactions and mechanisms for SIST were discussed.

Key words TiAl alloy strain induced structure transition phase transformation interfacial structure

1 INTRODUCTION

Now it is becoming apparent that the mechanical properties of two-phase γ-TiAl alloy depend strongly on the optimization of the designed microstructures which can be produced by controlled processing and appropriate alloying[1]. Recently, development of microstructures by appropriate thermo-mechanical treatment (TMT and TMP etc.) is under intensive investigation so as to develop balanced improvements of the properties[1]. A microstructure consisting of refined grain and controlled full lamellar(FL) is often required for a balanced improvement in ductility, toughness and strength. Nevertheless, the interfacial structures and lamellar structure can also be changed significantly due to heavy deformation and simultaneous recovery or recrystallization during thermo-mechanical processing. Our publications[2-4] showed the evidences for a verity of hot deformation induced non-equilibrium twin boundaries and special γ/α interfaces in two-phase γ-TiAl alloy. The contribution of these non-equilibrium interfaces to the mechanical properties must be considered. The non-equiliblium interfaces mean that the structure of these interfaces are deviated from the normal structures of the twin boundaries and the γ/α interfaces in annealed two-phase γ-TiAl alloys.

Strain induced ordered-structure transition is an important phenomenon in ordered alloys. Recently it was reported the strain induced disordering and creep enhanced reordering even further transiting the ordered structure from B_2 to DO_3 in Fe_3Al alloys[5]. In TiAl, a few publications[6-11] showed the ordered structure transitions during deformation, such as γ → α, α → γ and γ → 9*R* long period structure. Our recent work indicated that all these strain induced phase transitions are common during hot deformation of two-phase TiAl alloys[3, 12-14]. Meanwhile our work indicated that the twinning deforma-

① Project 59331013 supported by the Natural Science Foundation of China Received Jun. 26, 1997

tion at various {111} planes become more easy to take place during hot deformation. The structure at the intersection between twins of different {111} planes is complicate. The ordered structure can be significantly changed near these intersections.

All these microstructure changes occurred during thermomechanical processing will give a significant effect on the deformation behavior and mechanical properties of TiAl alloy. Fundamentally, we are just beginning to sufficiently understand the essential aspects of these important microstructure changes. This paper will briefly introduce these structure transitions during hot deformation in a two-phase TiAl alloy. Possible mechanisms of these structure transitions are also discussed.

This paper leads to note the strain induced structure transition (SIST) of a dual-phase TiAl alloy, including the structure changes in non-equilibrium α/γ interfacial boundaries and twin structures, and more fine phase constituents.

For multi-components TiAl alloys the changes in ordered atomic distribution should be considered. For example, our research has indicated that Nb in TiAl randomly occupies the sublattice of Ti when the Nb content is lower, but appears a tendency of ordering distribution as the Nb content increases[18].

2 EXPERIMENTAL

The alloy investigated was two-phase TiAl alloy having 45% Ti, 45% Al and 10% Nb (mole fraction). It was prepared from high purity Ti(99.9%), Al (99.9%) and Nb(99.9%) by non-consumable electrode arc-melting in a purified argon atmosphere. The ingot was remelted four times to ensure a complete mixing for the consitituents. The thermomechanical treatment is a quasi-isothermal-forged processing. The as-cast ingot (300g) was wrapped in a steel foil and heated to 1 350 ℃ for 30 min and then quasi-isothermally forged. The temperature of forge hammer was 1050 ℃. The strain rate was about $5 \times 10^{-1}\ s^{-1}$. The deformation strain was greater than 40%. The forged ingot was cooled to room temperature in air.

For the HREM studies, slices about 0.2 mm in thickness were cut from the sample. The slices were mechanically ground to less than 0.1 mm in thickness and then thinned by twin jet polishing (using an electrolyte of 300 ml methoanol+ 175 ml butanol+ 30 ml perchloric acid) and/or ionmilling. HRTEM was performed in a JEOL-2000EX II electron microscope operating at 200 kV with a spherical aberration coefficient of 0.7 mm. Interfaces in the samples were examined in either ⟨110] or ⟨101] orientations with the α_2/γ interfaces edge on.

3 RESULTS AND DISCUSSION

3.1 Non-equilibrium twin boundaries and special γ/α interfaces

Fig. 1(a) shows an asymmetrical or partially coherent twin boundary with high density of ledges that are one or two atomic planes in height. The mean ledge spacing is only 3.6 nm. Such high density of ledges makes the twin boundary plane to rotate off the symmetry plane for 0.5~ 2°, resulting in the formation of partially coherent twin boundary. The dark contrast in front of the ledges reveals that high stresses exist at the ledges. Fig. 1(b) shows an asymmetrical γ_A/γ_D pseudo-twin interface with a large number of ledges. The γ-TiAl has a tetragonal $L1_0$ structure, and all the ⟨110⟩ directions are not equivalent. Therefore the orientation relationships between twins will give to six possible orientation variants. The symbols γ_A, γ_B, γ_C, γ_D, γ_E and γ_F are used to distinguish the six γ variants with [110], [$\bar{1}$10], [101], [$\bar{1}$01], [011], [0$\bar{1}$1] orientation respectively. The pseudo-twin boundary under equilibrium condition is not completely coherent due to the existence of crystal misfit between γ_A and γ_D. However, the density of ledge of this equilibrium pseudo-twin boundary is much less than that of the asymmetrical pseudo-twin boundary. Fig. 2 is a typical non-equilibrium semi-coherent γ/α interphase boundaries. This boundary between ledges still keep atomically flat and structurally coherent, but the density of the ledges in these α_2/γ interfaces is much higher than that in annealing alloys. The height of ledges always ap-

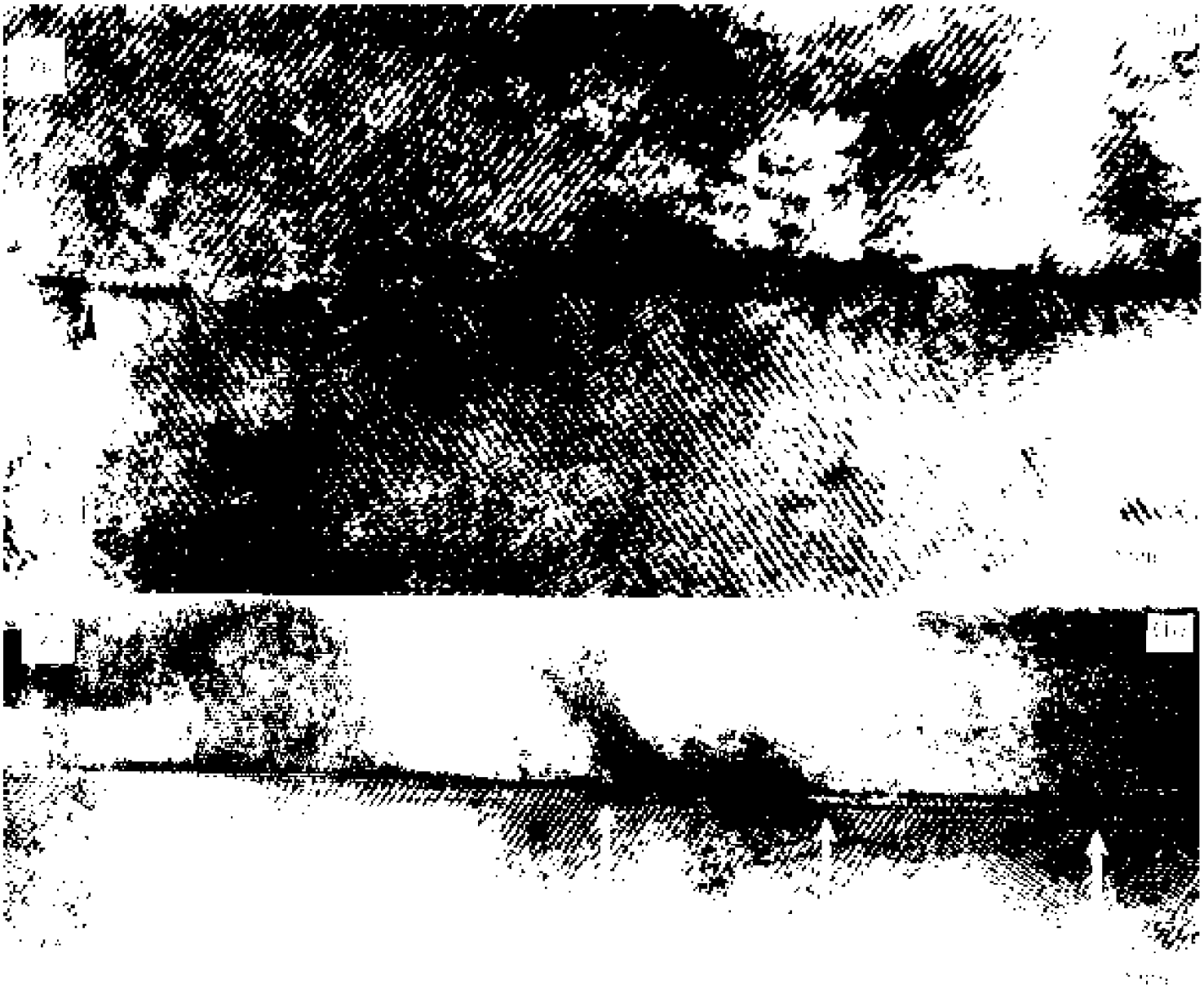

Fig. 1 Non-equilibrium interfacial structure of TiAl

proaches to the height of two $(0001)_{\alpha_2}$ planes. The dark contrast in front of the ledges reveals that high stresses exist at the ledges. The mean ledge spacing is less than 10 nm, which is much smaller than the ledge spacing of annealed alloys. Fig. 3 shows an interesting special γ/α interfaces. In the two-phase TiAl alloys, the orientation relations between neighboring α_2-Ti_3Al and γ-TiAl lamellae are well defined as $(0001)_{\alpha_2} \parallel \{111\}_\gamma$ and $\langle 11\bar{2}0\rangle_{\alpha_2} \parallel \langle 110\rangle_\gamma$ with the interface plane $(0001)_{\alpha_2}$ or $(111)_\gamma$. However, Fig. 3(a), (b) and (c) show the special γ/α interfaces that deviate from the normal crystal relation between γ/α phases. The orientation relation of $\langle 101\rangle_\gamma \parallel \langle 11\bar{2}0\rangle_{\alpha_2}$ between α_2 and γ remains unchanged, but the $(111)_\gamma$ is not parallel to the $(0001)_{\alpha_2}$ plane. The deviation angles between $(0001)_{\alpha_2}$ and $\{111\}_\gamma$ are 2.5, 8 and 18.5° respectively. The deviation angle has a significant influence on the interfacial structure. The larger the deviation angle is, the higher the ledge density is. The ledge spacing are 4.6, 1.8 and 1.0 nm for the deviation anlge of 2.5°, 8° and 18.5° respectively. In fact, when the deviation angle reaches 18.5°, the crystal relation between γ and α_2 phases has been changed to

Fig. 2 Non-equilibrium semi-coherent γ/α$_2$ interphase boundaries

[101]$_\gamma$ // [1120]$_{\alpha_2}$ and ($11\bar{1}$)$_\gamma$ // ($1\bar{1}00$)$_{\alpha_2}$. The interphase plane is not flat with high density of ledges, but is roughly parallel to (0001)$_{\alpha_2}$ plane and inclines to (111)$_\gamma$. A large lattice mismatch of 20% between $d_{(1100)\alpha_2}$ (= 0.288 nm) and $d_{(111)\gamma}$ (= 0.231 nm) can be accommodated by both high density of ledges and the special dislocation structure of interfaces. The dislocation structure of these ledges always contains 1/3[111] Frank partial dislocation that will be discussed next paragraph.

During thermodynamically-processing the moving dislocations in the γ lamellae may react with twin boundaries and α$_2$/γ interfaces, and/or can be absorbed by these interfaces, which results in the formation of non-equilibrium twin boundary and special α$_2$/γ interfaces. Since the twin's crystal relation must be kept, the main type of the non-equilibrium twin boundary is an asymmetrical twin boundary. However, since the deformation ability between γ and α$_2$ lamellar is different the deformation occurs mainly in γ lamellae may leads to rotate the γ lattice. Therefore, the normal crystal relation between α$_2$ and γ should be changed, resulting in the formation of both tilted and asymmetrical α$_2$/γ interfaces. This fact means that the α$_2$/γ interface is a more effective dislocation sink than the twin boundary.

3.2 Formation of 1/3[111] Frank partial dislocaitons at ledges

To follow the analysis procedures for drawing the Burgers circuits described by Howe *et al*[15], the characteristics of ledge dislocations in normal ledges can be determined to be 90° or 30° Shockley dislocation ledges. The Burgers vector of the 90° Shockley partial dislocation lies perpendicular to the [110] electron beam direction with 1/6[112], whereas for the 30° Shockley partial dislocation the Burgers vector lies at an angle of 30° to the electron beam and is either 1/6[211] or 1/6[121]. The unique characteristics of these hot deformation induced ledges, however, is the formation of 1/3[111] Frank partial dislocations. Fig. 4 is a typical example in which the 1/3[111] Frank partial dislocations are combined with Shockley partial dislocations. The ledge *C* in Fig. 4 can be determined as 90° Shockley dislocation + 1/3[111] Frank partial dislocation. The ledge *D* is a 30° Shockley dislocation+ 1/3[111] Frank partial dislocation. The formation of these 1/3 [111]

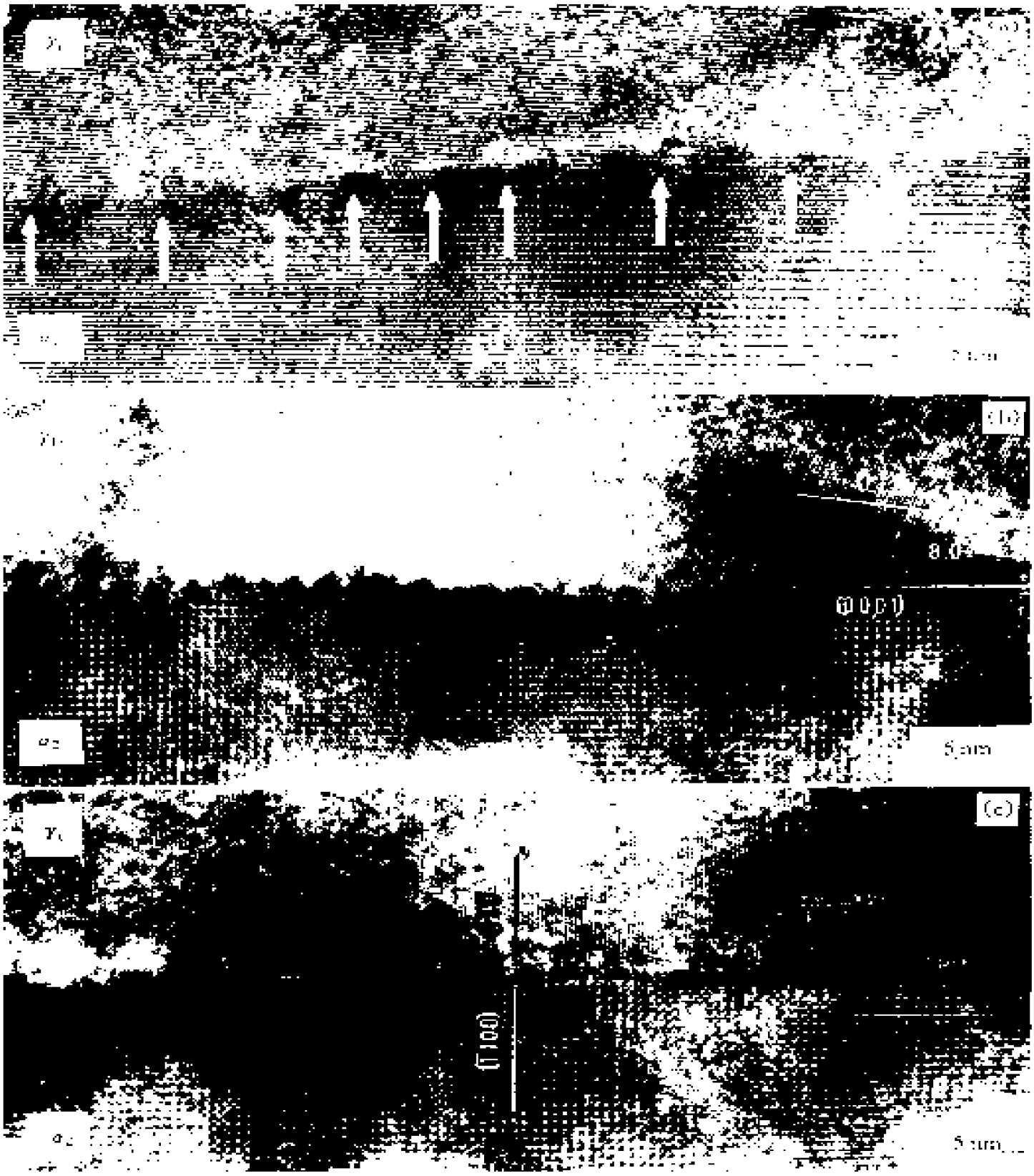

Fig. 3 Special γ/ α_2 interfaces that deviate from the normal crystal relation between γ/ α_2 phases at different tilt angles between (0001)$_{\alpha_2}$ and {111}$_{\gamma}$

(a) −25°; (b) −8°; (c) −18°

Fig. 4 HREM images of non-equilibrium γ/α$_2$ interfaces with 1/3[111] Frank partial dislocation

(a) —Ledge C-90° Shockley dislocation+ 1/3[111] Frank partial dislocation;
(b) —Ledge D-30° Shockley dislocation+ 1/3[111] Frank partial dislocation

Frank partial dislocations can also be considered as the results of introducing an extra half atomic plane (111) shown in Fig. 5. Both the special α$_2$/γ interfaces and non-equilibrium pseudo-twin boundary always contain the 1/3[111] Frank partial dislocations. These ledges are difficult to move at low temperatures, but at high temperatures the Frank partial dislocations may climb away from ledges.

A large number of glides in γ phase may lead to a tilt of γ lattice which must be accommodated by the formation of interfacial dislocations near the α$_2$/γ interface. The formation of 1/3[111] Frank partial dislocations exemplifies such important effect which effectively accommodates the tilt of $(111)_\gamma$ against $(0001)_{\alpha_2}$. In addition, the moving dislocations in the γ lamellae may slip to the α$_2$/γ interface and twin boundaries, and react with interfacial dislocations resulting in the absorption of the moving dislocations. These effects of dislocation traps of interfaces cause the change of interfacial structure, which leads to rotate off the symmetrical twin plane or the normal crystallographical relation of α$_2$/γ, $\langle 101]_\gamma \parallel \langle 1120\rangle_{\alpha_2}$ and $(111)_\gamma \parallel (0001)_{\alpha_2}$, resulting in the formation of semi-coherent α$_2$/γ interphase boundaries. The larger the deviation angle between γ and α is, the more the 1/3[111] Frank partial dislocations occur, and the more the moving dislocations absorb.

TiAl with $L1_0$ structure only can be twinned by the $\{111\}\langle 11\bar{2}]$ twinning mode, otherwise $L1_0$ structure no longer preserved. Therefore, the twinning dislocations are 1/6$[11\bar{2}]$ Shockley dislocations, which is well known that the possible moving dislocations during high temperature deformation are 1/2[110], [011] and 1/2[112]. Therefore, the moving dislocations may dissociate at interfaces by following reactions:

$$1/2[112] \rightarrow 1/6[112] + \text{SISF} + 1/6[112] + \text{SISF} + 1/6[112] \quad (1)$$

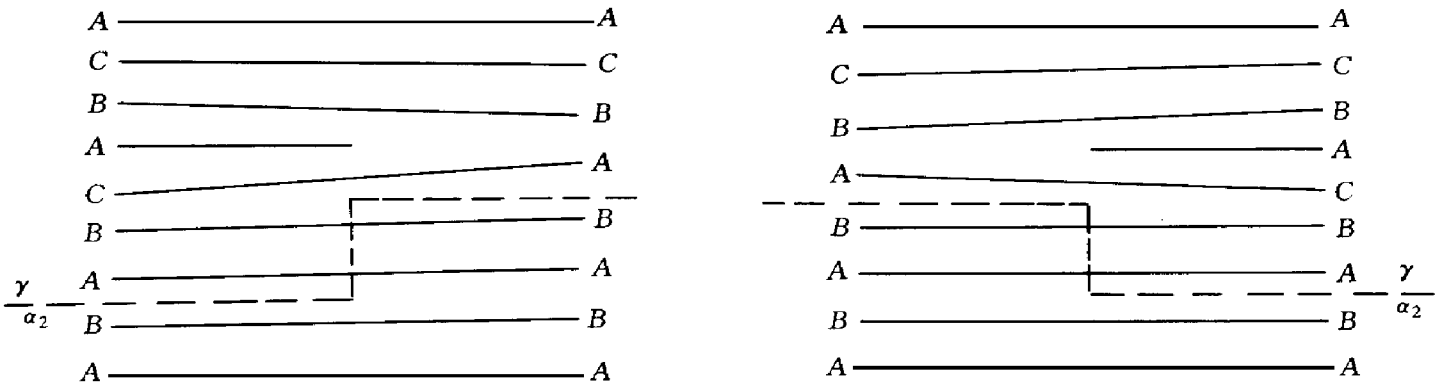

Fig. 5 Schematic diagram of 1/3[111] Frank partial dislocation at ledge

$$1/2[011] \rightarrow 1/6[121] + \text{SISF} + 1/6[\bar{1}12] \quad (2)$$

$$1/2[110] \rightarrow 1/3[111] + \text{SISF} + 1/6[11\bar{2}] \quad (3)$$

These dissociated dislocations can be absorbed by the interfaces, resulting in the formation of the ledges and/or 1/3[111] Frank partial dislocations. It is important to note that there is another way to form 1/3[111] Frank partial dislocations. The moving 1/2[110] dislocation reacts with 1/6⟨112⟩ Shockley partial dislocations at the interface as following:

$$1/2[110] + 1/6[\bar{1}\,\bar{1}2] \rightarrow 1/3[111] \quad (4)$$

The formation of ledges and 1/3[111] Frank partials at twin boundaries or α_2/γ interfaces is schematically described in Fig. 6. During hot deformation, the 1/3[111] Frank partial dislocations can move away from the ledges by climb, and react with another 1/6⟨112⟩ Shockley partial dislocation at the opposite interfaces as following:

$$1/3[111] + 1/6[11\bar{2}] \rightarrow 1/2[110] \quad (5)$$

This reaction results in an ordinary dislocation 1/2[110]. This may lead 1/2[110] gliding across the lamellae with a change of the interfacial structure (Fig. 6). Since burgers vectors of 1/3[111] and 1/6[11$\bar{2}$] in the reactions (3) and (5) are orthogonal and therefore the reaction results in neither increase nor decrease in the energy of the 1/2[110] dislocation, the driving force for the reactions (3) or (5) is thought to be originated from the release of the strain energy near the boundaries.

3.3 Strain induced *9R* structure

Fig. 7(a) shows a *9R* structure at a pseudo-twin γ_D/γ_A boundary. The *9R* structure locates at the end of the pseudo-twin boundary which can be imaged as a multiple height ledges. Fig. 7(b) shows a lamellar structure composed of four γ variants and *9R* structure. On the bottom of the figure, three γ variants $\gamma_C/\gamma_D/\gamma_C$ is in true twin relationship. On the upside of the figure, three γ variants $\gamma_B/\gamma_A/\gamma_B$ is also in true twin relationship. At the middle of the figure, there are two 120°-rotation type boundaries γ_A/γ_C and γ_B/γ_D. Two *9R* structures are formed in between of γ_B/γ_C pseudo-twin. The *9R* structure seems to locate at the multiple height ledges of the pseudo-twin boundary. In sum, the *9R* structure was always found to be formed at the multiple height ledges of either twin or pseudo-twin boundary, and parallel to the primary twin plane.

The *9R* structure can be considered to consist of a periodic array of hexagonal stacking faults on every third close-packed plane in a perfect FCC stacking sequence. The stacking sequence is *ABC/BCA/CAB*. Fig. 8 is the magnified photo of the *9R* structure in Fig. 7(b). Fig. 9 shows the selected area electron diffraction pattern(SADP). According to SADP, the orientation relationship between the *9R* structure and γ-TiAl matrix can be determined as following:

$$[010]_{9R} \parallel [101]_{\gamma},\ (001)_{9R} \parallel (111)_{\gamma}$$

The *9R* structure is an orthorhombic structure. Based upon the lattice parameter ratio given by Nishiyama and Kajiwara[16] for a perfect *9R* structure, $a : b : c = 1.732 : 1 : 7.348$, the unit cell parameters for the *9R* structure are

$$a = d_{(001)} = (\sqrt{6}/2)\, a_{\gamma} = 4.90\,\text{Å}$$

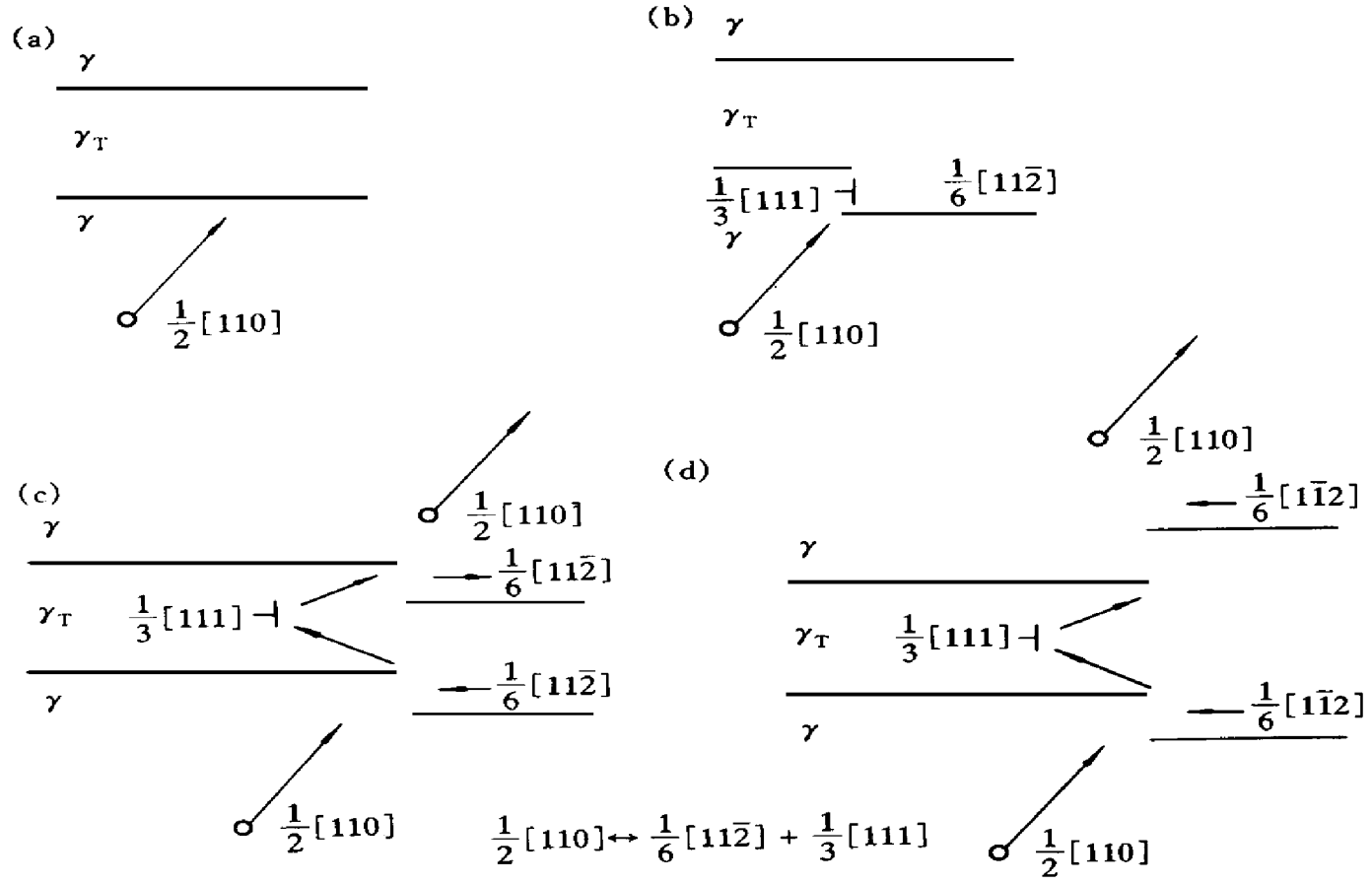

Fig. 6 Schematic diagram of formation of ledges at interfaces

(a), (b) —With 1/3[111] Frank partial dislocation; (c), (d) —Without 1/3[111] partial dislocation

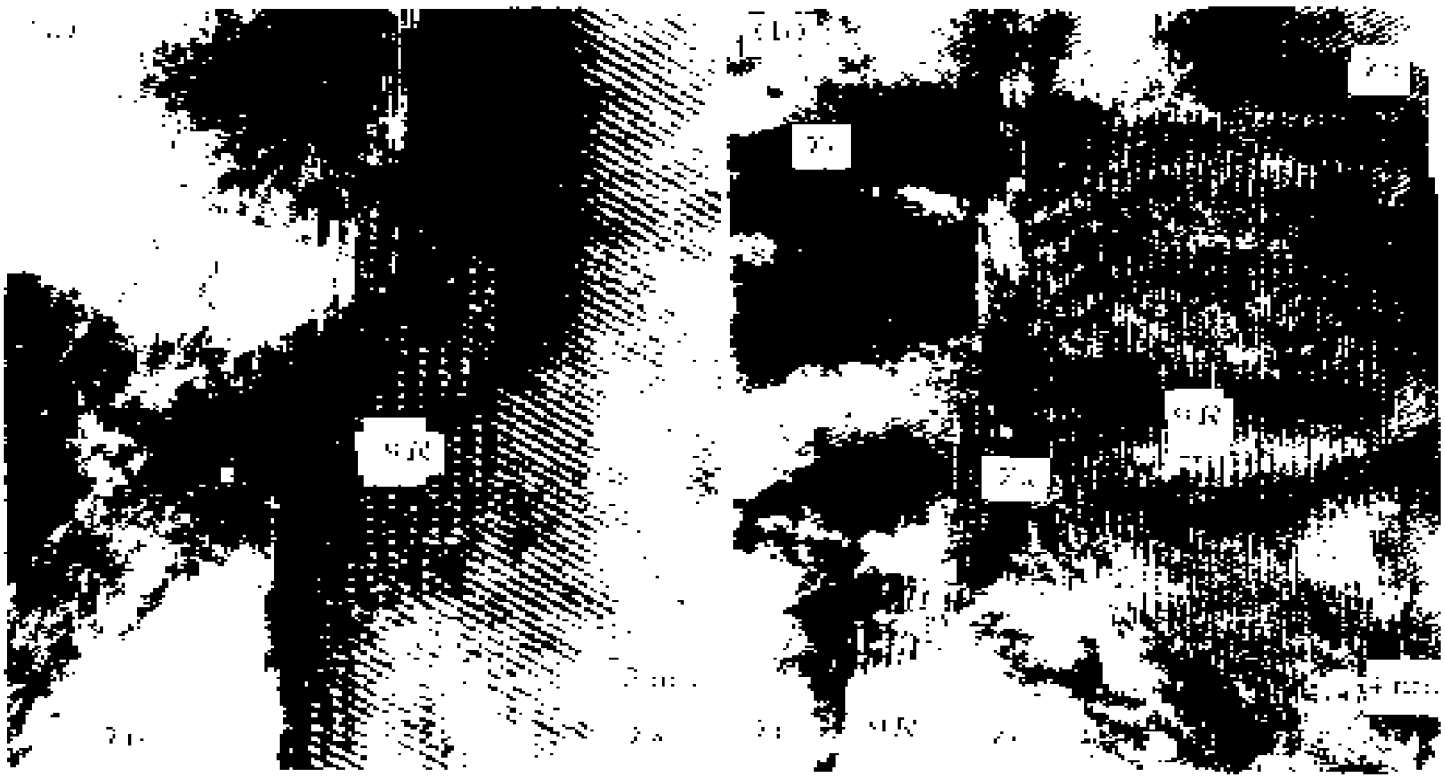

Fig. 7 HREM images of *9R* structure

(a) —Pseudo-twin boundary; (b) —Twin boundary

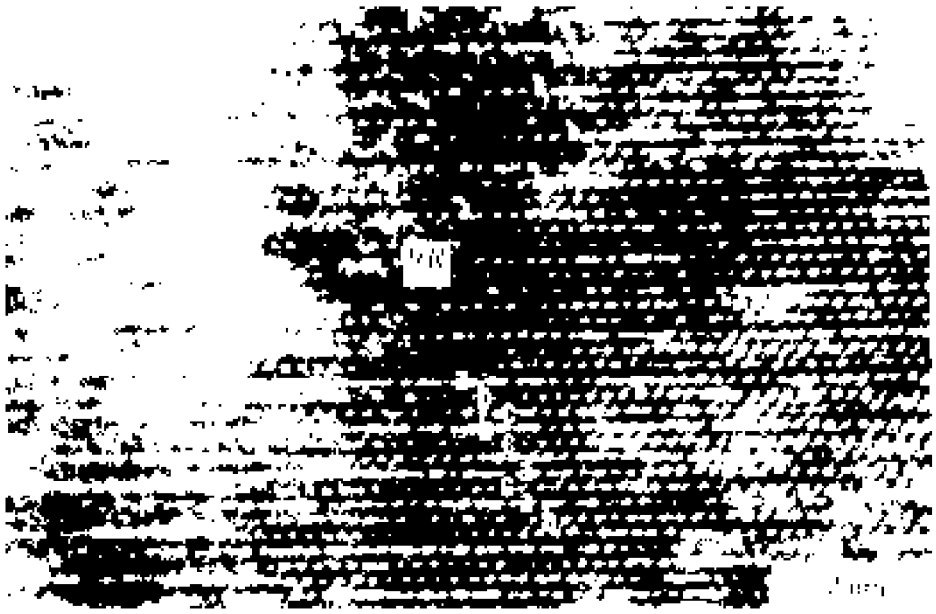

Fig. 8 Magnified photo of *9R* structure in Fig. 7(b)

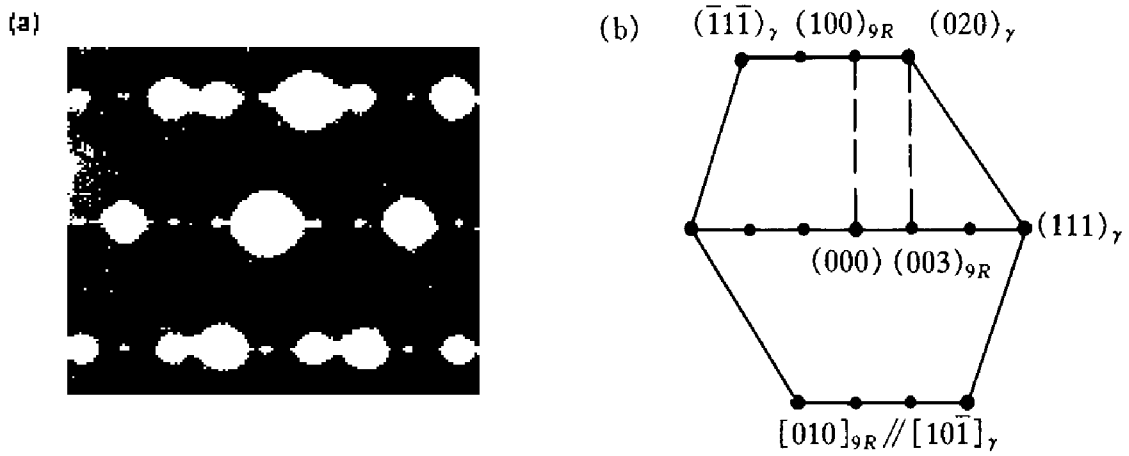

Fig. 9 Selected area diffraction pattern (SADP) of *9R* structure

$b = d_{(010)} = d_{(101)\gamma} = 2.82$ Å

$c = d_{(001)} = 9d_{(111)\gamma} = 20.8$ Å

Fig. 10 illustrates the atomic structure of the end of the twin boundary which can be imaged as a multiple height ledges of a non-coherent twin boundary viewed along a $[101]_M/[101]_T$ direction. Following the analysis procedure of the Read circuit construction for the determination of the Burgers vectors of the grain boundary dislocations[17], the interfacial dislocation for an ideal case is 1/6[112] Shockely partial dislocations. The spacing D between the interfacial Shockley partial dislocations is three $(111)_\gamma$ atomic planes, which meets the requirement for the formation of stacking faults every third close-packed planes. Therefore, the $9R$ structure can be produced. For normal case the interfacial dislocations contain 1/3[111] Frank partial dislocations. This may lead to form additional stacking faults randomly distributed on the close-packed planes of $9R$ structure.

3.4 Strain induced $\gamma \rightarrow \alpha_2$ phase transition

Fig. 11(a) shows a lamellar structure composed of $\gamma_C/\gamma_D/\alpha_2$, where the γ_D/α_2 interface is a deviating semi-coherent α_2/γ interfaces with deviation angle θ of 2.5°. Above this interface, a thin deformation-induced α_2 plate (here refered to as DI-α_2) with about 25 nm long and 2.5 nm thick forms in the γ_D lamellae, meanwhile the γ

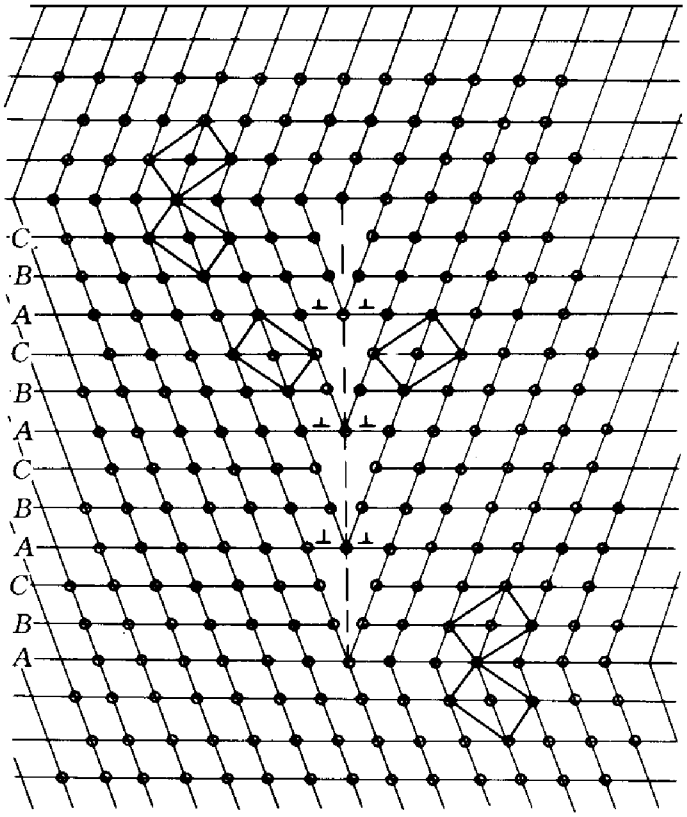

Fig. 10 Schematic diagram of atomic structure of a mutiple height ledge of a non-coherent twin boundary
(viewed along a $[101]_M/[101]_T$ direction)

lamellae between the α_2 lamellae and the DI-α_2 plate changes from γ_D to γ_B. Fig. 11(b) is a magnified photo of the region containing DI-α_2. Both the orientation relation between γ_B and α_2 and the orientation relation between γ_B and DI-α_2 are nearly exact $[110]_\gamma \parallel [1120]_{\alpha_2}$ and $(111)_\gamma/(0001)_{\alpha_2}$. A deviating angle θ of ~ 2.5° appears between the $(111)_{\gamma_D}$ plane and the (0001) DI-α_2. A similar deviating angle between $(111)_{\gamma_B}$ and $(111)_{\gamma_D}$ planes also appears. The 1/3[111] Frank partial dislocations are observed at both the γ_D/DI-α_2 interface and the γ_D/γ_B boundary. Fig. 12 shows a well-grown DI-α_2 plate near the deviating semi-coherent α_2/γ_D interface. It is about 5 nm thick and as long as the whole image. Also the γ phase between the α_2 lamellae and the DI-α_2 plate changes from γ_D to γ_B, and it is divided into many blocks by stacking faults of (111) planes which are either associated with a ledge at γ_B/DI-α_2 interface or suspended in the γ_B phase. The above observations show that the basic aspects of the formation of the DI-α_2 plate include following points:

(1) The formation of DI-α_2 always starts from the semi-coherent α_2/γ_D interface(the deviation angle is about 2.5°).

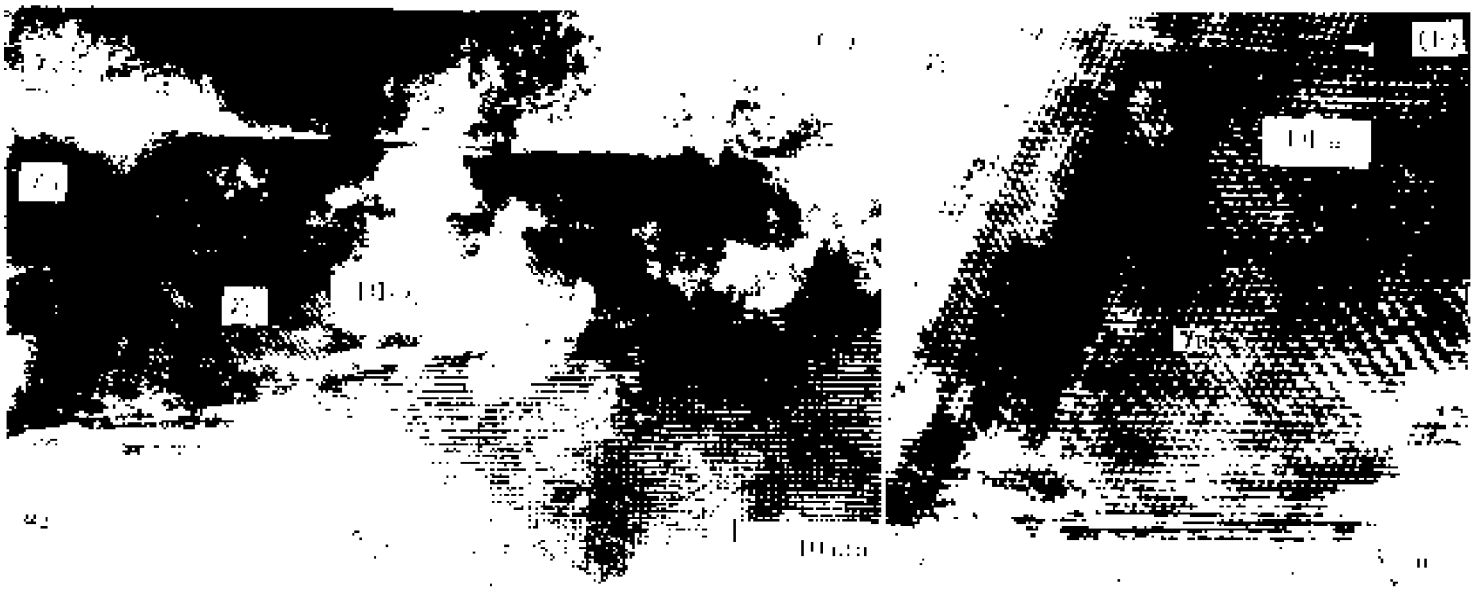

Fig. 11 HREM images of SIST
(a) —Strain induced $\gamma \rightarrow \alpha$ phase transition at a semi-coherent α_2/γ interfaces with deviation angle θ of 2.5°;
(b) —A magnification of region containing DI-α_2

Fig. 12 A well-grown DI-α_2 plate near deviating semi-coherent α_2/γ interface

(2) The interfacial dislocation always contains a 30° Shockley dislocation + 1/3[111] Frank partial dislocation. The Burgers vector of 30° Shockley partial dislocation is inclined at an angle of 30° to the electron beam, and it is either 1/6[$\bar{2}$11] or 1/6[$\bar{1}$21].

(3) The formation of DI-α_2 always accompanies the change of the γ variants, usually from γ_D to γ_B. Sometimes many stacking faults divide γ variant into many blocks.

During thermo-mechanical deformation, the interfacial dislocations of semi-coherent α_2/γ interfaces which are a kind of superdislocations of 1/2[011] are emitted, and slip on the ($\bar{1}$11) plane. Such a dislocation movement makes the γ variant change from γ_D to γ_B. After a short distance movement of this superdislocation, it may be separated into 1/3[111] + 1/6[$\bar{2}$11] partial dislocations because the ($\bar{1}$11) plane is not a primary slip plane and the movement of 1/2[011] dislocation on the ($\bar{1}$11) plane needs the rearrangement of the atoms. The 1/3[111] Frank partial dislocation can react with a common dislocation 1/2[$\bar{1}\bar{1}$0] on ($\bar{1}$11) plane and results in a 1/6[$\bar{1}$12] Shockley partial dislocation on (111) primary slip plane. The slip of this 1/6[$\bar{1}$12] Shockley partial dislocation on every other (111) plane leads to formation of the DI-α_2 phase.

3.5 Strain induced $\alpha_2 \rightarrow \gamma$ phase transition

Fig. 13(a) shows a α_2 lamellae that is separated into two parts by a deformation induced γ(DI-γ) plate. This DI-γ phase plate is formed at the deviating semi-coherent α_2/γ_D interface and penetrate into the α_2 phase. The orientation relation between the α_2 and the DI-γ plate is exactly $[1120]_{\alpha_2} \parallel [111]_{\gamma}$ and $(0001)_{\alpha_2} \parallel (111)_{\gamma}$. The (111) plane of γ_D and the (111) plane of DI-γ have an ~ 2.5° angle. Fig. 13(b) shows the 'head' part of the DI-γ plate. Very high stress exists at this area so that it is very difficult to obtain a distinct HREM image. At the 'head' of the DI-γ plate, it can also be seen that the $\alpha_2 \rightarrow$ DI-γ transition is accomplished by the travel of $a/3\langle 1010\rangle$ Shockley partials on alternate basal plane $(0001)_{\alpha_2}$.

The interfacial dislocations not only exist in γ phase but also in α phase. The interfacial dislocations in α_2 phase for a deviating semi-coherent α_2/γ_D interface is mainly the $a/6\langle 1120\rangle$. During deformation, the $a/6\langle 1120\rangle$ partials can be emitted from the interface and undergo a dissociation as following[18]:

$$a/6\langle 1120\rangle \rightarrow a/6\langle 1010\rangle + (\mathrm{APB} + \mathrm{SISF}) + a/6\langle 1010\rangle$$

The reaction occurs on every other α_2 basal plane. Then $a/6\langle 1010\rangle$ Shockley partials move in coordination into the α_2 phase on the α_2 basal planes, resulting in the structure change of α_2 to FCC. The stacking sequence of $(0001)_{\alpha_2}$ planes *ABAB* …… is altered to that of $(111)_{\mathrm{FCC}}$ *ABCABC* ……The nucleation of the DI-γ plate also can not be from α_2 / γ interface. In this

Fig. 13 HERM images showing DF γ in α_2 and γ TiAl

(a) —A DF γ plate in α_2 phase;
(b) —Head part of DF γ plate

case, the stacking fault plays an important role for nucleation and growth of DF γ plate.

4 CONCLUSIONS

The various strain induced phase transitions are closely related to the interface structure. The structure of ledges of interfaces is the most important factor.

The structure change during deformation for ordered alloys significantly influence the deformation behavior and mechanical properties. Basically, the dislocation emitting at crack tip is not the main factor to control the brittleness of normal intermetallic alloy systems, and the difficulty of dislocation movement often plays an important role in lowering the ductility. The strain induced structure transition is a significant aspect to understand the difficulty of dislocation movement.

REFERENCES

1 Kim Y-W. JOM, 1994, 46: 30.
2 Zhang L C, Wang J G, Chen G L *et al*. Intermetallics, 1997, 5: 289.
3 Chen G L, Wang J G, Zhang L C *et al*. Acta Metall Sinica, 1995, 8(6): 273.
4 Wang J G, Zhang L C, Chen G L *et al*. Acta Met Sinica, 1997, 10: 323.
5 Chen G L, Huang Y D, Yang W Y *et al*. In: Schneibel J H and Crimp M A eds, Processing, Properties and Application of Fe_3Al based aluminides. TMS, 1994: 131.
6 Appel F, Beaven P A and Wagner R. Acta Metall Mater, 1993, 41: 1721.
7 Feng C R, Michel D J and Crowe C R. Scripta Metall, 1989, 23: 241.
8 Feng C R, Michel D J and Crowe C R. Mater Sci Eng, 1991, A145: 257.
9 Gao Y, Zhu J, Shen H *et al*. Scripta Metall Mater, 1993, 28: 651.
10 Singh S R and Howe J M. Phil Mag Lett, 1992, 65: 233.
11 Zhang Y G, Ticheaar F D, Schapink F W *et al*. Scripta Metall Mater, 1995, 32: 981, 1995.
12 Wang J G, Chen G L, Zhang L C *et al*. Materials Letter, 1997, 31: 179.
13 Wang J G, Chen G L, Zhang L C *et al*. J Mater. Sci, in press, 1998.
14 Wang J G, Chen G L, Zhang L C *et al*. Scrip Met 1997, 37(2): 135.
15 Howe J M, Dahmen U and Gronsky R. Phil Mag, 1987, A56: 31.
16 Nishiyama Z and Kajiwara S. Jap J Appl Phys, 1963, 2: 478.
17 Hirth J P, Balluffi R W. Acta Metall, 1973, 21: 929.
18 Chen G L, Wang J G, Sun Z Q *et al*. Intermetallics, 1994, 2: 31.

(Edited by Huang Jinsong)